ELSEVIER

Journal of Atmospheric and Solar-Terrestrial Physics 67 (2005) 1448–1462

Journal of ATMOSPHERIC AND SOLAR-TERRESTRIAL PHYSICS

www.elsevier.com/locate/jastp

Correlations between earthquakes and anomalous particle bursts from SAMPEX/PET satellite observations

V. Sgrigna[a], L. Carota[b], L. Conti[a,*], M. Corsi[a], A.M. Galper[c], S.V. Koldashov[c], A.M. Murashov[c], P. Picozza[d], R. Scrimaglio[b], L. Stagni[e]

[a]*Dipartimento di Fisica and Sezione INFN, Università degli Studi Roma Tre, 84 Via della Vasca Navale, I-00146 Rome, Italy*
[b]*Dipartimento di Fisica, Università degli Studi di L'Aquila, Via Vetoio, I-67010 Coppito-L'Aquila, Italy*
[c]*MEPhI, Institute of Cosmic Physics, 31 Kashirskoe Shosse, 115409 Moscow, Russian Federation*
[d]*Dipartimento di Fisica and Sezione INFN, Università degli Studi "Tor Vergata", 1 Via della Ricerca Scientifica, I-00133 Rome, Italy*
[e]*Dipartimento di Ingegneria Meccanica ed Automatica, Università degli Studi Roma Tre, 79 Via della Vasca Navale, I-00146 Rome, Italy*

Received 11 August 2004; received in revised form 31 March 2005; accepted 7 July 2005
Available online 19 September 2005

Abstract

In the last decades, a possible influence of electromagnetic fields of seismic origin in the ionosphere–magnetosphere transition region has been reported in the literature. In recent years, a few space experiments also revealed anomalous bursts of charged particles precipitating from the lower boundary of the inner radiation belt. They were thought to be caused by low-frequency seismo-electromagnetic emissions. A recent study [Aleksandrin et al., 2003. Annales Geophysicae 21, 597–602] seems to confirm that these particle bursts have a short-term preseismic character. The particle longitudinal drift should enhance the detectability of preseismic particle bursts, thus magnifying their importance in earthquake prediction studies. This paper takes into consideration the method introduced by Aleksandrin et al. (2003) to carry out a deeper investigation on the subject. In this sense, a method for the temporal correlation between continental earthquakes with $M \geqslant 5.0$ and anomalous particle bursts collected by the PET-SAMPEX satellite mission is critically investigated and presented here. Several constraints and cuts have been applied to data in order to exclude, from the correlation, charged particles collected inside the SAA region and/or during ionospheric and magnetospheric perturbations caused by non-seismic sources. After the data have been detrended by these effects, a short-term seismic precursor of ~4 h is observed in the histogram of the time difference between the time occurrence of earthquakes and that of particle burst events. The best correlation is obtained only when considering high-energy electrons ($E \geqslant 4$ MeV) with pitch angles near the loss cone. Such a result confirms previous ones but also points out the importance of an ad hoc method of analysis. Results suggest the importance of coordinated and simultaneous ground-based and space investigations specifically dedicated to the subject. Also, a deeper investigation based on particle data prepared and analyzed as carefully as possible is requested to understand the physical mechanisms underlying the phenomenon under study.

Keywords: Earthquake precursors; Electromagnetic emissions; Radiation belt; Particle bursts; SAMPEX satellite

*Corresponding author. Tel.: +39 06 55177090; fax: +39 06 5579303.
E-mail addresses: sgrigna@fis.uniroma3.it (V. Sgrigna), contil@fis.uniroma3.it (L. Conti).

1364-6826/$ - see front matter © 2005 Elsevier Ltd. All rights reserved.
doi:10.1016/j.jastp.2005.07.008

1. Introduction

In recent years, interest has been increasing in the so-called seismo-electromagnetic perturbations consisting of broad-band (from $\approx$DC to a few tens of MHz) electromagnetic (EM) disturbances observed into the near-Earth's space, before, during, and after an earthquake (EQ). Characteristics and detectability of these perturbations have a very interesting and promising nature as a short-term EQ predictor. To detail such an indication, we outline in this section the main observations and models on the subject.

Ground-based measurements revealed slow electrotelluric and magnetic field variations (Johnston and Mueller, 1987; Varotsos et al., 1993) as well as preseismic ground potentials. The latter are generated as streaming potentials when saline water moving through porous rocks entrains ionic charges (Bernabé, 1998; Draganov et al., 1991), or through stress applied to rocks containing or not piezoelectric minerals as quartz (Bishop, 1981; Varotsos et al., 1997; Freund, 2002). The transmission of substantial stress over large distances has been debated (Geller, 1996; Sgrigna et al., 2002a; Sgrigna and Malvezzi, 2003).

Ground low-frequency (ULF/ELF) electromagnetic emission (EME) signals have also been documented in connection with relevant earthquakes (Kopytenko et al., 1993; Fraser-Smith et al., 1994; Ohta et al., 2001; Ismaguilov et al., 2001) and preliminary, though not exhaustive, explanations have been reported on the subject (Park et al., 1993; Merzer and Klemperer, 1997; Molchanov and Hayakawa, 1998; Surkov, 1999; Hayakawa et al., 2000).

More, in general, observations of local ground-based seismo-electromagnetic emissions (SEME) have been obtained on a larger (ULF–HF) frequency band (see, in addition to the above-mentioned authors, also Warwick et al., 1982; Oike and Ogawa, 1986; Johnston, 1997; Bella et al., 1998; Uyeda et al., 1999; Eftaxias et al., 2003).

Space observations of atmospheric and ionospheric perturbations over seismic regions have been reported and discussed on the occasion of several strong earthquakes (Gokhberg et al., 1989; Larkina et al., 1989; Parrot and Mogilevsky, 1989; Bilichenko et al., 1990; Serebryakova et al., 1992; Parrot et al., 1993; Chmyrev et al., 1997; Rodger et al., 1999; Lee et al., 2000; Pulinets et al., 2000; Hayakawa et al., 2002). Some authors dealing with statistical analysis of these space data gave indication to use caution on the subject (Henderson et al., 1993; Molchanov et al. 1993; Parrot 1999).

The above ground-based measurements, space observations, and related theoretical speculations, together with laboratory experiments (Nitsan, 1977; Yoshida et al., 1997; Freund, 2003) suggest different possible scenarios for the generation and propagation mechanisms of the broad-band seismo-electromagnetic perturbations (see also Dobrovolsky et al., 1989; Guo et al., 1994; Fenoglio et al., 1995; Molchanov et al., 1995; Teisseyre, 1997; Grimalsky et al., 1999; Sorokin et al., 2001; Gershenzon and Bambakidis, 2001; Fujinawa et al., 2002; Freund, 2003; Molchanov et al. 1993; Pulinets et al., 2000; Hayakawa et al., 2002). One of such scenarios is to consider these perturbations as due to SEME waves generated by preseismic sources and transmitted into the near-Earth space. Another one is to interpret EM disturbances as a secondary effect produced by other mechanisms induced by seismic activity.

On the basis of standard dilatancy–diffusion and crack-avalanche models (Myachkin et al., 1975), most of the investigators consider reasonable to assume the increasing and concentrating stress at depth in the fault asperity (preparation focal area) as a cause of the anelastic volumetric increase (*dilatancy*) of a relatively small portion of rock, and consequent rock dislocation and microfracturing.

As a result of these preseismic phenomena at depth, ground tilt and strain changes and electric and EM field variations are observed at the Earth's surface as a consequence of the field propagation from the hypocentral source, through the relatively highly elastic and conductive thin upper crust layer. During this propagation, the higher frequency content of the ULF-HF EME waves is attenuated and only ULF/ELF EME waves are supposed to reach the Earth's surface and enter into the near-Earth space, where they cause perturbations (total electron content (TEC) changes, ionospheric motions, joule heating, etc.) in the atmosphere and ionosphere (Molchanov et al., 1995; Ohta et al., 2001).

It has been shown (Areshidze et al., 1992; Bella et al., 1995; Guo et al., 1994; Molchanov and Hayakawa, 1998) that rock microfracturing releases gas (radon, helium) and causes electrical conductivity changes as a function of microcrack number and dimension and of pore fluids redistribution (saline pore fluids motion may cause the formation of intergranular water film). Recently, it has been proposed that also dry rocks can become a source of highly mobile electronic charge carriers, which increase the electric conductivity and may propagate through the rock as a charge cloud (Freund, 2002).

Fair weather currents have also been proposed to justify variations in the atmospheric conductivity profiles (Pulinets et al., 2000). Preseismic changes of the tropospheric conductivity profiles have also been associated with modifications of the spectral content of ELF-VLF radio noise during lightning discharges (Hayakawa et al., 2002). Molchanov et al. (1993), and Blanc (1985) demonstrated that EM disturbances observed in the upper atmosphere can also be the result of acoustic-gravity waves (AGW) in the ionospheric lower boundary due to seismic waves propagation.

From all the above-reported results, local deformation field, rock dislocation and microfracturing, gas emission, fluid diffusion, charged particle generation and motion, electrokinetic, piezomagnetic and piezoelectric effects, fair weather currents, quasi-electrostatic and EM channels of lithosphere–ionosphere interactions are the possible sources of preseismic EM perturbations.

The generation mechanisms and the propagation of these perturbations as well as their nature are out of the scope of the present paper, which is mainly focused in looking for the effects they produce in the radiation belt particles. Low-Earth-orbit (LEO) satellite observations seem to confirm the above-illustrated scenarios. Indeed, preseismic changes of electric and magnetic fields (Molchanov et al.1993; Parrot, 1994; Rodger et al., 1999) and of ionospheric plasma temperature and density (Parrot and Mogilevsky, 1989; Parrot et al., 1993; Chmyrev et al., 1997) have been observed from a few minutes to several hours prior to EQs of moderate or strong magnitude (generally greater than 4.0).

A relatively new result is that preseismic EM disturbances produced in a seismic area with one of the above-described mechanism, are thought to reach the inner Van Allen radiation belt, where they may interact with trapped particles (Galperin et al., 1992). In confirmation of this hypothesis, in the last two decades, a very interesting and new phenomenon has been observed in the ionosphere–magnetosphere transition region. It consists of anomalous particle fluxes detected by several space experiments and reconciled with the EQs occurrence (Galper et al., 1989; Voronov et al., 1990; Aleshina et al., 1992; Pustovetov and Malyshev, 1993). These particle fluxes are characterized by an anomalous short-term and sharp increase of high-energy particle counting rates (CRs). In the following, they are referred to as "particle bursts" (PBs). Most of PBs have been collected near the South Atlantic Anomaly (SAA) at altitudes generally between about 400 and 1200 km, by several satellites (Pustovetov and Malyshev, 1993; Ginzburg et al.,1994; Galper et al., 1995).

Larkina et al. (1989), and more recently, Sgrigna et al.(2002b) and Aleksandrin et al. (2003) also made attempts to confirm the preseismic character of these PBs, by using PBs–EQs statistical correlations, and under the hypothesis that preseismic ULF/ELF EME wave-trapped particle interaction may cause the precipitation of radiation belt electrons and protons.

With this purpose in mind several authors (Aleshina et al.,1992; Galperin et al., 1992; Galper et al., 1995; Krechetov, 1996) proposed that in a certain portion of the ionosphere–magnetosphere transition zone such a low frequency content of SEME radiation (from ~DC to some hundred Hz) can propagate as Alfven waves along the geomagnetic field lines. Near the radiation belt boundary, the waves may resonantly interact with trapped particles (electrons and protons from a few MeV to several tens of MeV) causing particle precipitation as a result of pitch angle diffusion. The lower limit of the above-mentioned portion of the ionosphere–magnetosphere transition zone (i.e., the altitude where preseismic ULF/ELF EME waves are captured in the geomagnetic field lines and, then, propagate as Alfven waves along these lines up to the inner radiation belt) has been estimated from PBs space observations and resulted to be around 300–500 km (Aleksandrin et al., 2003). A qualitative representation of this model is presented in Fig. 1.

Lifetime of PBs longitudinal drift is determined by the particle loss rate during particle interaction with the residual atmosphere of the Earth, and a lifetime of the order of several tens of minutes is obtained for electrons and protons of several tens of MeV (Walt, 1994). During this time, particles (drifting longitudinally) may move around the Earth along the L-shell corresponding to the EME ground source location (Aleshina et al., 1992; Galper et al., 1995). This is a crucial factor for a possible use of preseismic PBs as an EQ predictor, since the longitudinal drift makes the PB detection easier by particle detectors installed on board satellites. Another important factor is the opposite drift direction of positive and negative charged particles, which in principle could allow the location of EME wave–particle interaction zone (i.e., the PBs space source location) to be identified. Indeed, the above-reported LEO

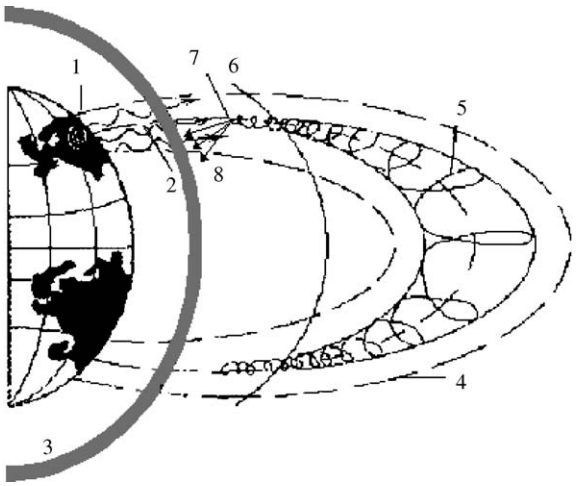

Fig. 1. Schematic representation in a meridian plane of the trajectories of charged particles trapped by the geomagnetic field lines. (1) Earthquake hypocentral "dilatant" area, where preseismic EME waves are emitted during the earthquake preparation, (2) EME-waves propagation from the preparation focal area to the ionosphere, (3) ionospheric interaction region, (4) geomagnetic field lines, (5) stationary trajectory of trapped particles, (6) stationary lower boundary of the radiation belt, (7) mirror points lowering, and (8) particle bursts precipitation and consequent longitudinal drift.

observations seem to confirm the possibility to detect these PBs caused by ULF SEME.

Also VLF EM waves were observed from Intercosmos-24 satellite measurements (Molchanov et al., 1993). Data collected by this mission demonstrated that ULF emissions of ~0.2 nT can penetrate through the ionosphere and interact with energetic protons of 0.5–5 MeV near the magnetic equatorial plane. As a consequence of this cyclotron interaction, the proton distribution function can become unstable for Cherenkov radiation of VLF waves in the frequency interval 0.1–20 kHz (Krechetov, 1996).

Nevertheless, there is still an open debate about the mechanism to be invoked in order to justify the entire phenomenon under study and, in particular, whether the very low amplitude ULF/ELF EM waves may reach the inner Van Allen radiation belt and cause the above-mentioned coupling phenomena. In fact, the electric and magnetic components of these EME waves are estimated to be of only some fraction of $mV/m(Hz)^{1/2}$ and of some fraction of $nT/(Hz)^{1/2}$ or less, respectively (Parrot et al., 1993).

But, as previously mentioned, both experimental evidence from several space missions and longitudinal drift character of precipitating PBs suggest a very exciting opportunity to detect preseismic PBs not only over seismic areas, but also at different longitudes along the perturbed L-shell. This enhances the PB detectability and its use as EQ precursor.

We think that this fascinating possibility demands further investigations on the subject. For this purpose, ground and space simultaneous and coordinated measurements must be carried out on the basis of information inferred from the above-reported results. Within this framework, multi-instrument and dedicated space missions with suitable orbital and instrumental characteristics are necessary and, in particular, a valid and ad hoc method for PBs–EQs correlation must be accomplished.

For this purpose, three space projects have been proposed in recent times: the DEMETER, ARINA, and ESPERIA missions. The polar mission DEMETER (Parrot, 2002) has been developed by the French Space Agency (CNES) and is more oriented to wave investigation. On the contrary, the polar ARINA experiment (Sgrigna et al., 2002b) is only devoted to particle measurements, and has been realized jointly by the Moscow Engineering Physics Institute (MEPhI) and the University of Rome, "Tor Vergata" (Picozza, 2003). ESPERIA is an equatorial mission planned and designed on the basis of a Phase A Study (Sgrigna, 2001) for the Italian Space Agency (ASI) and may be considered as a second generation of the DEMETER concept.

Aleksandrin et al. (2003) first pointed out a possible PBs–EQs correlation, which gave useful indications on a possible short-time (a few hours) preseismic character of PBs. They performed data analysis on particle data collected from space experiments Gamma-1, Maria-2, Electron, and Proton Electron Telescope (PET) carried out on board of MIR orbital station and METEOR-3, GAMMA and SAMPEX satellites, respectively. What is lacking now is an ad hoc methodology for testing correlations of similar quality, and a deeper knowledge of the physical mechanisms underlying the phenomenon under study.

The aim of the present paper is to give additional, more detailed, and complementary information to the promising results of Aleksandrin et al. (2003). At this purpose an ad hoc method for PBs–EQs spatial and temporal correlation will be proposed by emphasizing some critical aspects of data processing and measurement methodology. For comparisons we will apply our analysis to the same Solar Anomalous and Magnetospheric Particle Explorer (SAMPEX) level-2 data (Lennard et al., 2000) already used by Aleksandrin et al. (2003). In this way, we can also perform a check of our method and give useful information for its possible further optimization.

The paper is organized as follows. Sections 2 and 3 illustrate the mission characteristics required for the study and the consequently selected SAMPEX/PET space experiment and database. In Section 4 are discussed selection criteria and related cuts applied to data. The PBs–EQs correlation and relative statistical significance are performed and discussed in Section 5. Conclusions are reported in Section 6.

2. Selection of a suitable space mission for the study: the SAMPEX/PET mission

To perform a suitable PBs–EQs correlation, long time series of particle data are requested together with EQ parameters and information on magnetospheric perturbations caused by non-seismic sources. Moreover, it is reasonable to assume that most of preseismic PBs are detected by satellites whose orbit "skims" L-shells just beneath the lower boundary of the inner radiation belt. Previous results (Aleksandrin et al. 2001) indicate an orbit between around 500 and 1000 km of altitude as the most suitable for the study. Besides, high-energy particles which exhibit a relative long-time longitudinal drift are required. Previous results (Molchanov et al., 1993) and simple estimates (Aleshina et al., 1992) also indicate the use of data collected by a particle detector for electrons with $E_{e-} > 5$ MeV and protons with $E_{p+} > 50$ MeV, an energy resolution better than 5 MeV, time resolution less than 15 s, and angular resolution better than 5°. Finally, a large angular acceptance of the detector is needed to have significant statistics and to collect particles with pitch angle near the drift loss cone.

No dedicated and suitable space mission is available with these characteristics. Nevertheless, when considering all the above-listed conditions, only the SAMPEX NASA satellite, with on board the PET detector, is found to be an acceptable (though not optimal) mission for the study.

3. SAMPEX-PET mission and database

The main characteristics of the SAMPEX mission (Baker et al., 1993; Cook et al., 1993) are reported in Table 1. The PET instrument consists of an array of silicon solid-state detectors that identifies electrons and protons. PET channel Level-2 data available for the study (Lennard et al., 2000) are reported in Table 2. It can be seen from Table 2 that in PEN and RNG channels, electrons and protons are not separated, and PLE and PHI channels too consist of low-energy protons (i.e., particle with short-time longitudinal drift).

Table 1
Main characteristics of the SAMPEX/PET mission

Orbit altitude	520–670 km
Orbit inclination	82°
PET Pointing modes	ORR, MORR, 1 RPM (see text)
Time interval under study	from July 1992 to December 1999

Table 2
PET channel Level-2 data available for the study

Particles	Energy (MeV)	Geometric factor (cm^2 sr)	Channel
Protons	28–60	1.5	PHI
Protons	19–28	1.65	PLE
Electrons	2–6	1.65	ELO
Electrons	4–15	1.5	EHI
Electrons	4–30	—	EWG
Protons	>60	0.4	RNG
Electrons	>15		
Protons	>85	0.25	PEN
Electrons	>30		

Moreover, EWG channel exhibits a poor statistic due to a low geometric factor. Then, only Level-2 PET data from EHI and ELO channels can be considered for the study. But EHI channel exhibits a better event statistics than ELO one and has electrons with greater energy than those of ELO channel. So, it must be expected that EHI electrons are the best set of data for our study.

Level-2 PET data consist of CRs integrated over 30 s. In the following, CRs of electron channels EHI and ELO are referred to as CREHI or CRELO, respectively. Unfortunately, particle pitch angle data are unknown from the PET database where only α_{PET} (angle between the detector yaw axis and magnetic field direction) values are reported. This indicates that satellite PET-pointing modes influence the analysis (see, Tables 1 and 3, and Fig. 2).

As shown in Tables 1 and 3, SAMPEX/PET has operated with three different pointing programs: original Orbit Rate Rotation (ORR), Modified Orbit Rate Rotation (MORR), and 1 Rotation Per Minute (1 RPM). During the ORR-pointing mode, the PET yaw axis is substantially radial to the Earth. So, PET may detect particles with pitch angle in a wide range and, in particular, also in the loss cone (precipitating particles) or near it. On the contrary, in the MORR mode, the detector yaw axis is fundamentally perpendicular to the geomagnetic field lines, since it was implemented mainly to study particles with pitch angle near 90° (trapped particles). Measurements for α_{PET} values far from 90° are performed in periods during which PET yaw axis is parallel to the geomagnetic field (B), when $B > 0.3$ G, and perpendicular to it, when $B < 0.3$ G. Finally, in the 1 RPM mode, the α distribution is flat since the PET yaw axis, rotating continuously at 1 RPM, allows the particle detection at any pitch angle value. This is well illustrated by the four bottom panels of Fig. 2.

As specified in Table 3, CRs PET-data were classified in four time periods corresponding to the different pointing modes illustrated above. In Table 3, daily data collected during optimal device working conditions (here referred to as "good days") and detected with good quality flag according with the SAMPEX weekly instrument status report, are reported (http://nssdca.gsfc.nasa.gov/anon_dir/active/SAMPEX/SAMPEX_OPP.TXT).

Table 3
PBEHI and PBELO catalogues for the four time periods corresponding to the different SAMPEX pointing modes

Pointing mode	Period (MM/ DD/YY)	# "Good days"	# CR	# CR per day	# PBEHI	# PBELO
ORR	01/24/93–05/26/94	247	211603	857	1734	1259
MORR (1)	05/27/94–05/07/96	691	373976	541	3957	1848
1 RPM	05/08/96–05/06/98	677	195187	288	1253	485
MORR (2)	05/07/98–12/16/99	543	179457	330	1628	698

MORR (1) and MORR (2) identify two different time periods of observation but with the same (MORR) pointing program.

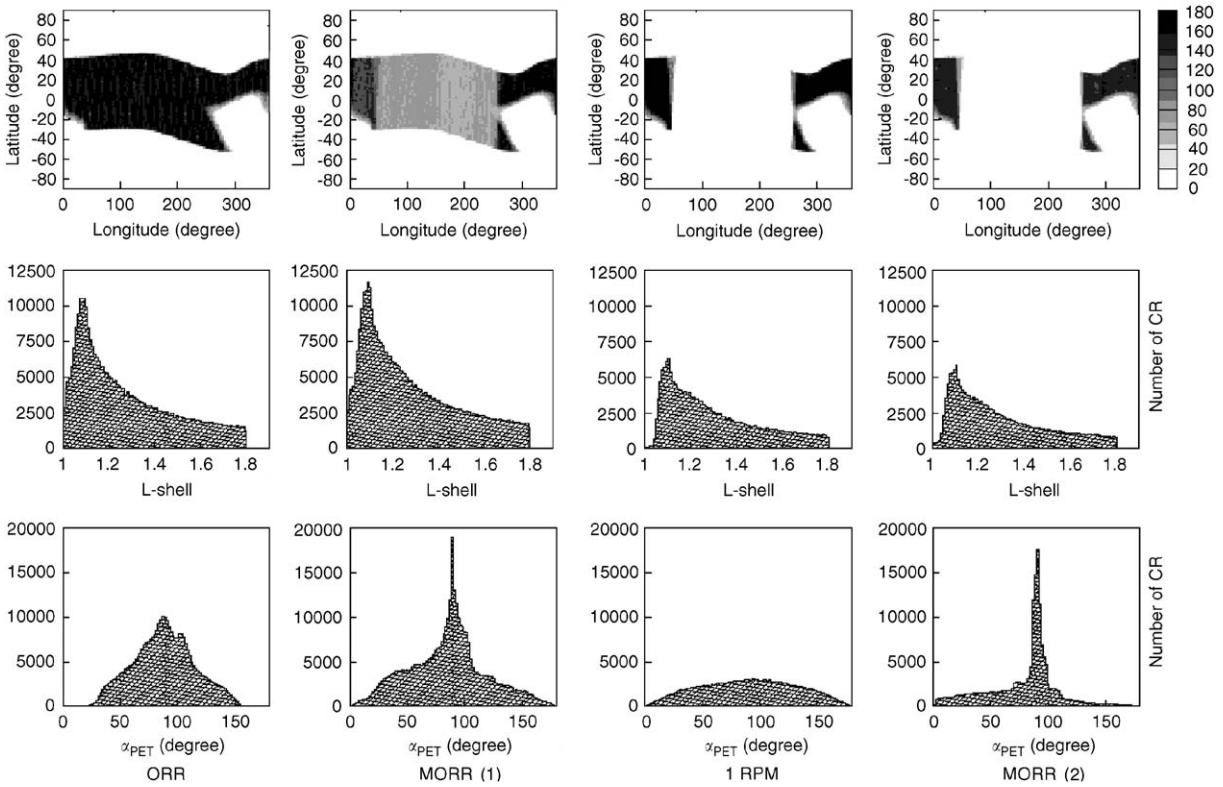

Fig. 2. Distribution of PET measurements for the different pointing time modes. Data have been collected in the $1.0 < L < 1.8$ interval. In the top line, the geographic distributions of CRs are reported. In the second and third (bottom) lines, the CRs distributions vs. L-shell and α_{PET}, respectively are shown.

The four panels in the top line of Fig. 2 show the geographic distribution of CRs measurements performed during each pointing mode.

During the MORR (1) mode, a non-homogeneous CRs geographical distribution due to scanty PET measurements performed in the longitude interval [50°–270°] is evident. PET measurements are further extremely reduced in this longitudinal interval during the 1 RPM and MORR (2)-pointing programs. In correspondence with the latter two periods, an abrupt decrease is observed in the CRs distribution vs. L, for $L \sim 1.0$–1.3 (second line of Fig. 2). The four panels in the bottom line of Fig. 2 clearly confirm that the α_{PET} distribution is pointing program dependent.

On the basis of all the above mentioned, it is evident that ORR mode is the most suitable pointing program to detect the maximum number of precipitating particles.

4. Selection criteria for the EQs and PBs populations to be correlated

In the following two sub-sections we will detail and clarify conditions for cuts applied to data in order to select EQs and PBs populations to be correlated.

4.1. EQs selection

Most of the seismic EME observations reported in the literature are generally associated with moderate and strong ($M \geqslant 4.0-5.0$) shallow earthquakes (Pustovetov and Malyshev, 1993). Then, earthquakes with magnitude $M \geqslant 5.0$ and hypocentral depth < 100 km ($\approx$lithospheric depth) have been selected for the study (USGS, 2003). Moreover, for a more restrictive selection, oceanic crust earthquakes have been rejected (Oike and Ogawa, 1986, Galper et al., 1989; Parrot, 1994), although an absorption of EME waves in the oceanic water is questionable (Ismaguilov et al., 2001).

Seismic EME wave–particle interaction zone is not yet exactly predicted by theory. According to Galper et al. (1995), and Aleksandrin et al. (2001, 2003), we have assumed that such a zone may extend at altitudes between $\sim$100 and $\sim$1200 km. L-shell values corresponding with PBs (L_{PB}) coincide with those of the PET position. On the contrary, we must estimate L-shell values corresponding with the interaction zone between trapped particles and preseismic EME waves (L_{EME}). For each selected EQ, L_{EME} has been defined by projecting the hypocentral area at an altitude over the

Earth's surface corresponding with the above-assumed EME wave–particle interaction zone (Pustovetov and Malyshev, 1993). As a first attempt, we have calculated L_{EME} by IGRF2000, at a reference altitude $z = 400$ km, and have considered such a reference altitude as a model-dependent and tuneable parameter.

Note that most of the EQs are located in the equatorial zone within a latitude interval of $\pm 30^{\circ}$, and that a variation of the hypocentral area projection altitude between 100 and 1200 km results in a corresponding L_{EME} uncertainty (ΔL_{EME}) of about 0.1.

4.2. PBs selection

As described in the introduction section and also shown in Aleksandrin et al. (2003), in general PBs are particle fluxes characterized by an anomalously sharp increase and time duration of a few ten seconds. That is, in a sequence of CRs, each one having a duration of 30 s, we observe a PB as an increase in the number of detected particles. The duration of this time series of data is relatively short, since it only consists of several CRs. The 30 s temporal resolution of Level-2 PET-data does not allow characteristic PB events to be individually observed. Then, only an anomalous deviation from the statistical distribution of the 30 s integrated CRs can be identified. These PB events are defined beginning from CRs (Table 3) detected at known L-shell and α_{PET} values.

On the ground of all these considerations, PBs have been defined with respect to a {L, α_{PET}} daily background matrix constructed as follows. L-shell and B values corresponding with each particle detection position have been calculated by the IGRF2000. Since most of the L_{EME} and L_{PB} distributions are included within $L = 1.8$ and zones with $L_{EME} < 2.0$ are mostly supposed to be affected by EME preseismic waves, we have restricted our analysis to L-shell values in the interval 1.0–1.8.

Then, we have divided the α_{PET} range (0–180°) into 12 steps of 15° each and the L-shell range (1.0–1.8) into 8 steps of 0.1 each. For each cell of the $\{L,\alpha_{PET}\}$ matrix, we have used the daily CR distribution as a reference background for estimating PBs. The L and α_{PET} step widths have been defined considering the amplitude of particle flux changes and the exiguous number of available daily measurements. Statistical tests performed on daily CRs pointed out a Poisson distribution of CRs for each $\{L,\alpha_{PET}\}$ matrix cell. Therefore, we have defined PBs as those CRs which assume values greater than those of the relative $\{L,\alpha_{PET}\}$ background matrix, and which probability (p) to be a Poisson fluctuation is less than an assigned threshold value (we choose $p < 0.01$).

Since the lower boundary of the inner radiation belt varies with time, it (and in particular the SAA region) has been determined yearly by the IGRF2000. The SAA region has been excluded from the study and only data collected during periods characterized by a geomagnetic index value $A_p < 20$ or in absence of ionospheric disturbances (SID = 0) have been included in the analysis. This is in order to separate ionospheric and magnetospheric perturbations produced by external sources (sun and cosmic rays) from those caused by EQs.

The number of PBEHI and PBELO data are reported in Table 3. In the $L = 1.0-1.8$ interval, both PBEHI and PBELO distributions vs. L agree with the CR's ones (Fig. 2 and 3), for the four different SAMPEX/PET-pointing modes. This seems to indicate that PBs selection has not introduced evident systematic errors.

5. PBs–EQs spatial and temporal correlation

As mentioned above, precipitating particles drift longitudinally around the Earth along a fixed L-shell, which being not modified by the EME-particle interaction is known through the satellite co-ordinates and geomagnetic field value. Then, the calculated L_{PB} value is model independent. On the contrary, also as discussed in sub-section 4.1, the estimated L_{EME} value is model dependent.

Due to previous results (Aleksandrin et al., 2003) and by basing on the possibility that wave–particle interaction may take place within the lower boundary altitude of the inner radiation belt (ranging between ~100 and 1200 km), only data with $\Delta L = |L_{EME} - L_{PB}| < 0.1$ have been considered for the PBs–EQs correlation (Table 4). Within this $\Delta L = 0.1$ interval, L_{PB} values range from -0.08 to $+0.03$, since we used $z = 400$ km as a reference altitude for the L_{EME} definition.

Then, we calculated the time difference $\Delta T = T_{EQ} - T_{PB}$, between the universal times of origin of EQ (T_{EQ}) and PB (T_{PB}) events, respectively. To perform a significant statistical analysis (see the following section) the PBs–EQs temporal correlation has been carried out in a time window of $\Delta T_{max} = \pm 3$ days, centered around each PB event.

The precipitated PBs propagating under the radiation belt experience an increasing scattering with distance, and this causes a consequent particle diffusion in the medium (Galper et al., 1989 and Voronov et al., 1990). Then, according to Galperin et al. (1992) and Aleksandrin et al. (2003), a cut was applied to the mirror point altitude (H_{MIRR}) in order to restrict areas for PBs acceptance. By considering the SAMPEX orbit altitude (500–600 km), this cut was assumed as 400 km $< H_{MIRR} < 900$ km. We estimated H_{MIRR} values by the IGRF2000 model and averaged them over the whole time period 1992–1999.

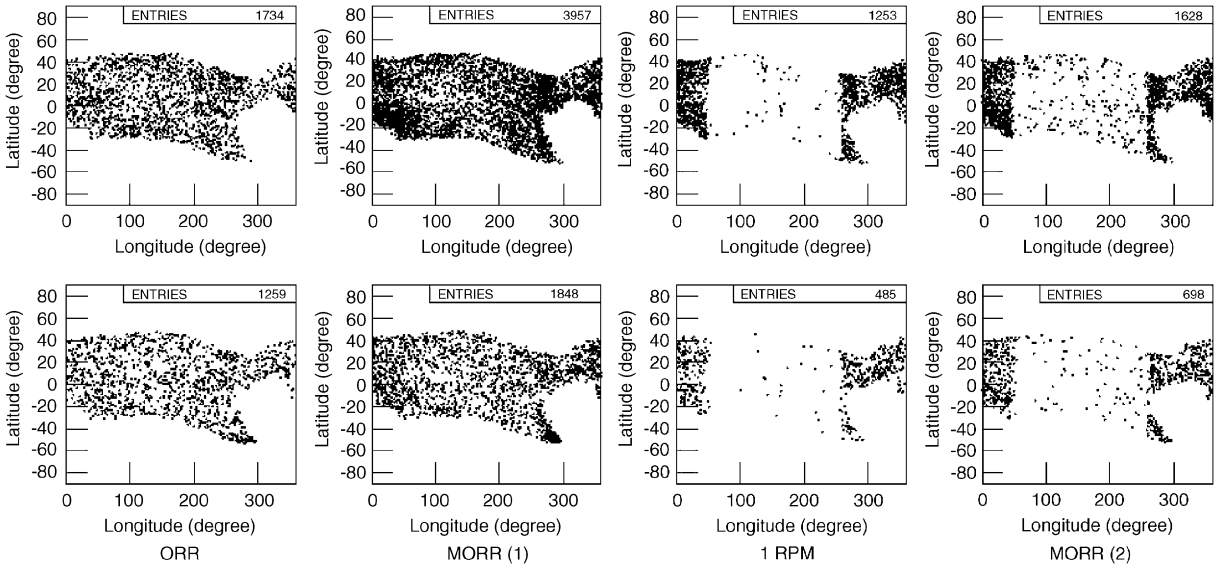

Fig. 3. Geographic distributions of PBEHI (top panels) and PBELO (bottom panels) data in the $1.0 < L < 1.8$ interval and for the four different pointing modes.

Table 4
Cuts applied to data for selecting EQs and PBs populations to be correlated

EQ event selection	PB event definition
$M \geqslant 5.0$	CRs = particle flux measurements integrated over 30 s
Hypocentral depth $h < 100$ km	CR daily background matrix $\{L, \alpha_{PET}\}$:
No EQs in the oceanic crust	$1.0 \leqslant L_{PB} \leqslant 1.8$ (L-step = 0.1)
$L_{EME} \sim L_{z=400\,km}$	$0^\circ \leqslant \alpha_{PET} \leqslant 180^\circ$ (α_{PET} − step = 15°)
	Poissonian cut: $p < 0.01$
	No measurements in the SAA region
	$A_p < 20$
	SID = 0
EQ–PB correlation	
$H_{MIRR} \approx 400-900$ km	
$\lvert H_{MIRR} - H_{SAMPEX} \rvert > 30$ km	
$\Delta L = L_{EME} - L_{PB} < 0.1$	
$\Delta T_{MAX} = (T_{EQ} - T_{PB})_{MAX} = \pm 3$ days	

Moreover, to exclude PBs collected inside the radiation belt (Aleksandrin et al., 2001), a distance greater than 30 km has been fixed between PBs detection altitude (H_{SAMPEX}) and H_{MIRR}. This restriction works near the SAA, the China anomaly (Arkani-Hamed et al., 1988) and, more in general, in areas where the satellite trajectory does not tend to skim L-shells, but cuts them.

In Table 4 ,selection criteria and related cuts discussed above and applied to data for the PBs–EQs correlation have been summarized.

Finally, to look for a possible maximum peak in the $\Delta T > 0$ region (a positive peak indicates that PB events statistically precede, in time, EQs occurrence), a histogram of the $\Delta T = T_{EQ} - T_{PB}$ frequency distribution has been constructed with data collected during each PET-pointing mode.

Such a maximum positive peak has been observed only when considering PBEHI data obtained during the ORR mode (Fig. 4). In this mode, 1734 PBEHI events have been selected from 211603 CR counting increments (see Table 3). This peak is evident near $\Delta T = 4$ h and includes 31 events. The ΔT frequency distribution of Fig. 4 has a standard deviation $\sigma = 3.5$ and background mean $\langle N \rangle = 15.5$. The confidence level of the peak is 4σ

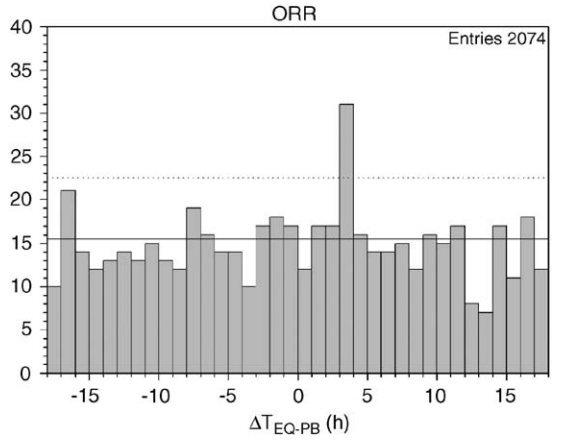

Fig. 4. Histogram of the $\Delta T_{\text{EQ-PB}}$ temporal correlations between PBEHI and EQs for the ORR PET-pointing mode. Only during this pointing period, a significant peak is evident at $\Delta T = 4$ h, demonstrating that only in this case PBs statistically precede EQs, thus indicating a preseismic character. A time window of 18 h has been used only for graphical representation. The horizontal solid and dotted lines indicate the mean amplitude of each distribution and the mean + 2 standard deviation units, respectively.

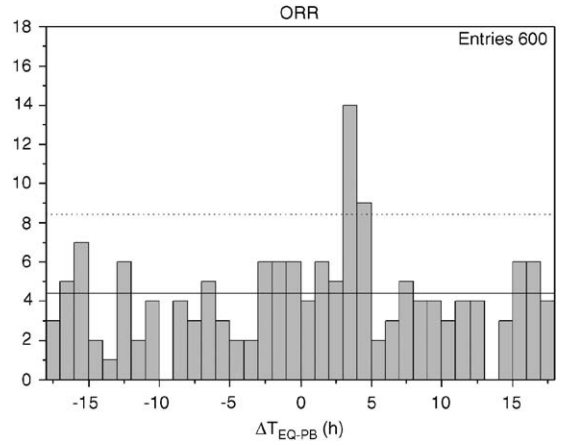

Fig. 5. Histogram of the $\Delta T_{\text{EQ-PB}}$ temporal correlation between EQs and PBEHI data (detected at $\alpha_{\text{PET}} < 70^{\circ}$ and $\alpha_{\text{PET}} > 110^{\circ}$) for the ORR PET-pointing period. As in Fig. 4, also in this case, but with a better signal-to-noise ratio, a peak is evident at $\Delta T = 4-5$ h only with data collected during the ORR-pointing mode, indicating that PBs statistically precede EQs, i.e., PBs exhibit a preseismic character. The horizontal solid and dotted lines indicate the mean amplitude of each distribution and the mean + 2 standard deviation units, respectively.

(i.e., the peak is 4σ out of mean) and only this peak exceeds the level of two standard deviation units (dotted line in Fig. 4). A bin step (τ) of 1 h has been used. For a better graphical representation, the histogram is reported with a time window of ± 18 h.

An increase of the peak statistical significance (i.e., of the signal-to-noise ratio) in the ORR histogram of Fig. 4 has been obtained by excluding from the data charged particles with $\alpha_{\text{PET}} \approx 90^{o}$ (trapped particles). In Fig. 5, an example in which such an improvement is obtained by excluding PBs detected in the α_{PET} range $70^{\circ} < \alpha_{\text{PET}} < 110^{\circ}$ is reported. In this case, the histogram of the ΔT frequency distribution is characterized by two maximum peaks at $\Delta T = 4-5$ h (including 25 events), $\sigma = 2.0$, and background mean $\langle N \rangle = 4.4$. As in Fig. 4, only these peaks exceed the level of two standard deviation units. Therefore, 25 PBEHI are connected with 19 EQs. The maximum peak at $\Delta T = 4$ h (including 14 events) is 4.5σ out of mean.

Contrary to the results from ORR data, no correlation is obtained (i.e., no relevant peak is observed) when considering data collected in the other MORR (1), MORR (2), and 1 RPM-pointing periods (Fig. 6) or when taking into account PBELO data. The good correlation with seismicity obtained only using ORR PBEHI data confirms results reported in the paper of Aleksandrin et al. (2003), but also gives an additional information.

In fact, in our study, results have demonstrated also a dependence on the particle energy and on the PET yaw axis position with respect to the geomagnetic field lines. This is a very important and useful information for defining a correct detector-pointing mode and particle selection in future missions. Results obtained here have shown to be stable under a little variation (lesser than 5%) of applied cuts.

5.1. Statistical considerations on the ΔT distribution

The confidence level ($n\sigma$) of the peak in the histogram of the ΔT frequency distribution is defined as

$$n\sigma = \frac{N_{\text{MAX}} - \langle N \rangle}{\sqrt{\langle N \rangle}}, \tag{1}$$

where n is an integer, σ the standard deviation, N_{MAX} the number of events in the peaks of ΔT histograms, and $\langle N \rangle$ is the average value of the histogram.

The behavior of such a confidence level vs. ΔL and vs. z (see, Table 4) has been analyzed in a previous paper (Aleksandrin et al., 2003). It was found that highest values of the confidence level (up to six standard deviations) are obtained when $|\Delta L| \sim 0.07$. For smaller $|\Delta L|$ values, a reduction of EQs–PBs correlation events and, hence, a reduction of the peak amplitude is observed. Also larger $|\Delta L|$ values (say, greater than 0.5), including into the statistics a greater number of EQs, increase the background events in the statistics and produce a decrease of the peak confidence level. These results, together with considerations reported above,

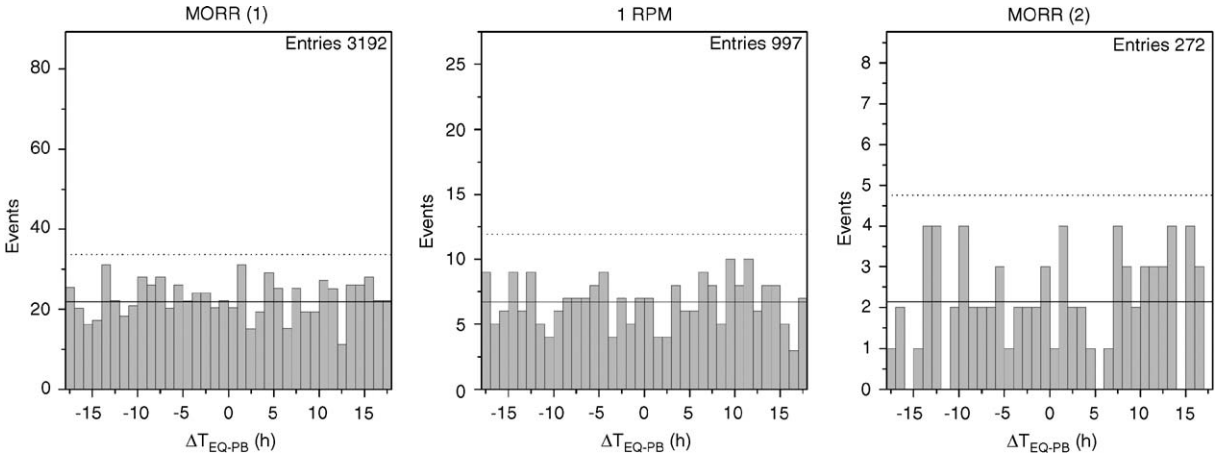

Fig. 6. Histograms of the ΔT_{EQ-PB} temporal correlation between EQs and PBEHI data (detected at $\alpha_{PET} < 70^{\circ}$ and $\alpha_{PET} > 110^{\circ}$) for the three MORR (1), MORR (2), and 1RPM-pointing periods. Contrary to what obtained with data collected during the ORR period (Figs. 4 and 5), no correlation is observed in these cases. A time window of 18 h is used only for graphical representation The horizontal solid and dotted lines indicate the mean amplitude of each distribution and the mean + 2 standard deviation units, respectively.

seem to justify ΔL cuts shown in Table 4 and applied to data.

Concerning the optimization of the ΔT histogram construction, we have to take into account that the theoretical data distribution is unknown and the experimental one is very sensitive to the ΔT bin step (τ), because of the relatively low statistics. The background level and the evidence of a temporal correlation peak are affected by the choice of the maximum time window (ΔT_{max}) between EQs and PBs events.

To optimize the histogram construction, we used two statistical methods: the Cross-Validation test (Rudemo, 1982) and the Stability Test (CV-G method) (Simonoff and Frederic, 1997).

The Cross-Validation test allows to find the optimal τ bin step, for which the experimental histogram $f_{exp}(x)_{\tau}$ is close point by point to the true density function $f(x)$, by minimizing the integrated squared error:

$$\int [f_{exp}(x)_{\tau} - f(x)]^2 \, dx \int [f_{exp}(x)_{\tau} - f(x)]^2 \, dx = \int f^2_{exp}(x)_{\tau} \, dx - 2 \int f_{exp}(x)_{\tau} f(x) \, dx + \int f^2(x) \, dx. \quad (2)$$

The first term on the right can be exactly computed as h is changed; the third term is ignored, since it does not change with h, whereas the second integral is proportional to the average height of the histogram. It is not valuable since $f(x)$ is unknown. For the second term, Rudemo (1982) suggests to costruct N histograms excluding one datum per time (repeating N times for each data point) and to average the N histogram evaluations. Then, expression (2) becomes

$$\int f^2_{exp}(x)_{\tau} \, dx - \frac{2}{N} \sum_{i=1}^{N} f^i_{exp}(x_i) = \frac{2}{(N-1)\tau} - \frac{N+1}{N^2(N-1)\tau} \sum_k c_k^2, \quad (3)$$

where $f_{exp}(x) = c_k/(N\tau)$ with $\{c_k\}$ bin counts in the histogram.

The Stability Test uses the stability index G to measure the similarity of the histograms resulting from all possible anchor position choices, for fixed bin width τ. A global quantity that is sensitive to changes in the shape of the density (Scott, 1992) is

$$S = \int \left(\frac{df}{dx} \right)^2 dx = \frac{\sum_k (c_{k+1} - c_k)^2}{N^2 \tau^3}. \quad (4)$$

For a fixed τ value, we calculate S_i for $i = 1, \ldots, M$, with M anchor positions. To check if the $\{S_i\}$ set is highly variable (suggesting instability), a variant of the G index (Marshall and Olkin, 1979) can be used. We define

$$q_i = \sum_{j=1}^{i} S_j / \sum_{m=1}^{M} S_m, \quad (5)$$

where $S_{(j)}$ is the jth order statistic, for $j = 1, \ldots, M$, and $q_0 = 0$. The pairs $\{j/M, q_j\}$ draw a curve in the unit square and we define the stability index G as twice the area below this curve: $G \in (0, 1]$ and values greater than 0.85 are usually interpreted as representing stable bin widths.

An optimal bin width τ must satisfy both the two statistical criteria. We have validated the CV-G method by many tests with random data generated by various density functions and we applied it to the SAMPEX/PET data analysis, changing the histogram window $\Delta T_{\max}$ from 10 h to 250 h (with steps of 1 h) and the bin width τ from 30 s to 10 h (with steps of 10 min).

We found that a bin width $\tau \sim 1-3$ h and a temporal window $\Delta T_{\max} \approx 150\,h$ have to be chosen to estimate a correlation between PBs and EQs in a range of few hours.

The histograms we illustrated in the previous section were obtained following this procedure. We choose a ΔT bin step of 1 h because we are looking for short-time precursors, and studied temporal correlation between PBs and EQs in a time window of ± 3 days to perform a more significant statistical analysis.

6. Discussion and conclusions

Although low-frequency EMEs have been observed on the ground and in space before strong EQs, their preseismic character and postulated contribution to the lithosphere–ionosphere interactions is far from a final experimental confirmation. Also the postulated preseismic character of anomalous fluxes of radiation belt particles are hotly debated. As a contribution to this debate, an attempt of correlation between anomalous CRs (PBs) from SAMPEX/PET satellite data and selected EQs has been carried out.

At this purpose, a specific method of data analysis has been proposed. For comparisons, we applied our method to the same SAMPEX Level-2 data (Baker et al., 1993) already used in a previous work by Aleksandrin et al. (2003). In this way, we could check the method and give useful information for its possible further optimization. In fact, the detailed description of the performed analysis and related comparison also reveals some critical aspects of data processing and measurement methodology.

The results we have obtained give indication for a deeper investigation on the subject in order to understand the physical mechanisms involved in the phenomenon under study with particular emphasis on the efficiency of wave–particle interaction mechanisms. At this purpose, better high-quality particle data are necessary. Our results also point out the importance of suitable particle detector-pointing modes and specific detector physical and technical characteristics.

Concerning the method of analysis, several constraints and cuts have been applied to data in order to exclude, from the correlation, PBs collected inside the SAA region and/or during ionospheric and magnetospheric perturbations caused by non-seismic sources (background rejection).

Thresholds for EQs magnitude and hypocentral location have been assumed as well as a suitable altitude for the EME-particle interaction zone.

In these conditions, PBs of precipitating high-energy radiation belt electrons are demonstrated to precede, statistically by some hours, the occurrence of moderate and strong EQs. No correlation was found between PBs and other noise sources, as solar and magnetospheric activities, that could, in principle, cause particle precipitation.

The above positive PBs–EQs correlations, and in particular the PBs short-time preseismic character confirm those carried out with a similar method and reported in previous papers. But our results also add useful information on a few critical aspects about methods of investigation and data analysis. In fact, the best correlation has been obtained only when using high-energy particles and with pitch angle near the loss cone, thus indicating that a relatively long-term longitudinal drift and the detector-pointing mode are critical factors for revealing these EQ precursors. As a confirmation, negative results were observed in the case of not suitable satellite-pointing programs, low-energy particles, and in presence of a poor statistics.

PBs and EQs with $|\Delta L| = |L_{\mathrm{EME}}\text{-}L_{\mathrm{PB}}| < 0.1$ have been selected. The best estimate of the ΔL value was performed by considering the reference altitude z (then, L_{EME}) as a free parameter and recalculating histograms for different ΔL values. A decrease in the confidence level of the peak in the ΔT histogram was observed for $|\Delta L| < 0.03$ and $|\Delta L| > 0.1$. This was explained with the reduction in the number of PBs events and with the massive presence of EQs with associated L_{EME} values far away from L_{PB} ones.

The fact that we did not find a significant correlation at low-energy level could mean either that there are few seismic-induced precipitations of low-energy particles or that the observation and correlation techniques are less efficient than those concerning high-energy particles. In general, we cannot state that particles are disturbed by SEME waves at any energy and frequency value. We think that precipitation takes place only at resonant frequencies. Moreover, for low-energy PBs, the observation of precipitation is not guaranteed due to the short-time duration of the longitudinal particle drift, and to the drift dispersion in the arrival time of particles at SAMPEX/PET. For these reasons, low-energy PBs seem not to be very effective as seismic precursors. That is why we think that positive PBs–EQs correlations obtained only at high energies could indicate a selectivity order in the phenomenology under study. On the contrary, should correlations be observed at any energy level, this could be a sign of an accidental phenomenon.

Of course EQs are not the only possible source but an adding source of particle precipitation correlations. That is why we took into consideration many non-seismic

causes such as X-rays, solar emission bursts, and geomagnetic storms. Geomagnetic (A_p) and solar activity (SID) indices have been used to monitor these events. None of these sources give evident correlation except two geomagnetic storms caused by strong interplanetary shock waves (February 21th, 1994 and August 20th, 1998) accompanied by significant injection in the magnetosphere of energetic electron. For this reason, PBs detected in these two periods have been excluded from the study. The geomagnetic micropulsation activity is strongly connected to A_p changes (Smirnova, 1999); then, a further analysis has been performed comparing the temporal behavior of PBEHI and geomagnetic A_p index. No evident correlation has been found in this case.

Results suggest that in addition to a suitable detector-pointing mode and a long-term particle longitudinal drift, another important factor to use PBs as EQ precursors is the simultaneous PBs detection of both high-energy electrons and protons. In fact, in principle, we think that the opposite drift direction of positive and negative charged particles and the expected drift dispersion in the arrival time of these particles (the temporal profile is expected to be dependent upon the separation longitude of EQ and satellite) could allow the location of SEME wave–particle interaction zone (i.e., the PBs space source) to be identified. To check this hypothesis, a new study is needed and with better high-quality data, which are not available from PET instrument.

Results of the present study, although not exhaustive for a complete confirmation of the preseismic character of EME waves detected in the ionosphere–magnetosphere transition zone, give useful and adding information with respect to the rare previous studies of similar quality.

A few LEO satellite observations seem to confirm the possibility to detect PBs caused by preseismic ULF/ELF EME waves, corroborating the importance of a scientific project for a suitable method of data analysis and for a dedicated space mission devoted to identify PBs and SEME short-term EQ precursors.

In this regard, the DEMETER mission (Parrot, 2002) of the French Space Agency (CNES) has been launched on June 2004 and the ARINA (Picozza, 2003) experiment (sponsored by an international consortium led by the University of Rome, "Tor Vergata", Italy) will be launched on September 2005. A new mission (ESPERIA) is under a selection procedure by the Italian Space Agency (ASI). The ESPERIA Phase A Study has already been performed by a consortium of several teams led by the University Roma Tre, Italy (Sgrigna, 2001).

Acknowledgment

We thank the two unknown reviewers for their constructive comments and suggestions, which gave us the opportunity to improve the paper.

References

Aleksandrin, S.Yu., Forzan, F., Galper, A.M., Grishantzeva, L.A., Koldashov, S.V., Maslennilov, L.V., Murashov, A.M., Picozza, P., Voronov, S.A., 2001. Origin of high-energy charged particle bursts in the near-Earth space. In: Proceedings of the ICRC 2001, pp. 4144–4147.

Aleksandrin, S.Yu., Galper, A.M., Grishantzeva, L.A., Koldashov, S.V., Maslennikov, L.V., Murashov, A.M., Picozza, P., Sgrigna, V., Voronov, S.A., 2003. High-energy charged particle bursts in the near-Earth space as earthquake precursors. Annales Geophysicae 21, 597–602.

Aleshina, M.E., Voronov, S.A., Galper, A.M., Koldashov, S.V., Maslennikov, L.V., 1992. Correlation between earthquake epicenters and regions of high-energy particle precipitations from the radiation belt. Cosmic Research 30 (1), 79–83.

Areshidze, G., Bella, F., Biagi, P.F., Caputo, M., Chkuaseli, V., Della Monica, G., Ermini, A., Manjgaladze, P., Melikadze, G., Sgrigna, V., Slavina, L., Zilpimiani, D., 1992. Anomalies in geophysical and geochemical parameters revealed in the occasion of the Paravani ($M = 5.6$) and Spitak ($M = 6.9$) earthquakes (Caucasus). Tectonophysics 202, 23–41.

Arkani-Hamed, J., Zhao, S.K., Strangway, D.W., 1988. Geophysical interpretation of the magnetic anomalies of China derived from MAGSAT data. Geophysical Journal of the Royal Astronomical Society 95, 347–459.

Baker, D.N., Mason, G.M., Figueroa, O., Colon, G., Watzin, J.G., Aleman, R.M., 1993. An overview of the Solar Anomalous and Magnetospheric Particle Explorer (SAMPEX) Mission. IEEE Transactions on Geoscience and Remote Sensing 31, 572–574.

Bella, F., Biagi, P.F., Caputo, M., Cozzi, E., Della Monica, G., Ermini, A., Plastino, W., Sgrigna, V., 1995. Helium content in thermal waters revealed in the Caucasus from 1985 to 1991 and their correlations with the seismic activity. Tectonophysics 246, 263–278.

Bella, F., Biagi, P.F., Caputo, M., Cozzi, E., Della Monica, G., Ermini, A., Plastino, W., Sgrigna, V., 1998. Field strength variations of LF radio waves prior to earthquakes in Central Italy. Physics of the Earth and Planetary Interiors 105, 279–286.

Bernabé, Y., 1998. Streaming potential in heterogeneous network. Journal of Geophysical Research 103, 20827–20841.

Bilichenko, S.V., Iljin, F.S., Kim, E.F., Pokhotelov, O.A., Puschaev, P.P., Stanev, G.A., Streltsov, A.V., Chmyrev, V.M., 1990. ULF response of the ionosphere for earthquake preparation processes. Doklady Akademii Nauk USSR 311, 1077–1080.

Bishop, J.R., 1981. Piezoelectric effects in quartz-rich rocks. Tectonophysics 77, 297–321.

Blanc, E., 1985. Observations in the upper atmosphere of infrasonic waves from natural or artificial sources: a summary. Annales de Geophysique 3, 673–688.

Chmyrev, V.M., Isaev, N.V., Serebryakova, O.N., Sorokin, V.M., Sobolev, Ya.P., 1997. Small-scale plasma inhomogeneities and correlated ELF emissions in the ionosphere over an earthquake region. Journal of Atmospheric and Solar-Terrestrial Physics 59, 967–974.

Cook, W.R., Cummings, A.C., Cummings, J.R., Garrard, T.L., Kecman, B., Mewaldt, R.A., Selesnick, R.S., Stone, E.C., Baker, D.N., von Rosenvinge, T.T., Blake, J.B., Callis, L.B., 1993. PET: a proton/electron telescope for studies of magnetospheric, solar, and galactic particles. IEEE Transactions on Geoscience and Remote Sensing 31, 565.

Dobrovolsky, I.P., Gershenzon, N.I., Gokhberg, M.B., 1989. Theory of electrokinetic effects occurring at the final stage in the preparation of a tectonic earthquake. Physics of the Earth and Planetary Interiors 57, 144–156.

Draganov, A.B., Inan, U.S., Taranenko, Y.N., 1991. ULF magnetic signatures at the Earth surface due to the ground water flow: a possible precursor to earthquakes. Geophysical Research Letters 18, 1127–1130.

Eftaxias, K., Kapiris, P., Polygiannakis, J., Peratzakis, A., Kopanas, J., Antonopoulos, G., Rigas, D., 2003. Experience of short term earthquake precursors with VLF–VHF electromagnetic emissions. Natural Hazards and Earth System Sciences 3, 217–228.

Fenoglio, M.A., Johnston, M.J.S., Byerlee, J.D., 1995. Magnetic and electric fields associated with changes in high pore pressure in fault zones: application to the Loma Prieta ULF emissions. Journal of Geophysical Research 100, 12951–12958.

Fraser-Smith, A.C., McGill, P.R., Helliwell, R.A., Villard Jr., O.G., 1994. Ultra-low frequency magnetic field measurements in southern California during the Northridge earthquake of 17 January 1994. Geophysical Research Letters 21, 2195–2198.

Freund, F., 2002. Charge generation and propagation in igneous rocks. Journal of Geodynamics 33, 543–570.

Freund, F., 2003. On the electrical conductivity structure of the stable continental crust. Journal of Geodynamics 35, 353–388.

Fujinawa, Y., Takahashi, K., Matsumoto, T., 2002. Modeling confined pressure changes inducing anomalous electromagnetic fields related with earthquakes. Journal of Applied Geophysics 49, 101–110.

Galper, A.M., Dimitrenko, V.B., Nikitina, N.V., Grachev, V.M., Ulin, S.E., 1989. Interrelation between high-energy charged particle fluxes in the radiation belt and seismicity of the Earth. Cosmic Research 27, 789.

Galper, A.M., Koldashov, S.V., Voronov, S.A., 1995. High energy particle flux variations as earthquake predictors. Advances in Space Research 15, 131–134.

Galperin, Yu.I., Gladyshev, V.A., Jordjio, N.V., Larkina, V.I., 1992. Precipitation of high-energy captured particles in the magnetosphere above the epicenter of an incipient earthquake. Cosmic Research 30, 89–106.

Geller, R.J., 1996. Debate on VAN. Geophysical Research Letters 23 (whole issue 11), 45–46.

Gershenzon, N., Bambakidis, G., 2001. Modeling of seismo-electromagnetic phenomena. Russian Journal of Earth Science 3, 247–275.

Ginzburg, E.A., Malishev, A.B., Proshkina, I.P., Pustovetov, V.P., 1994. Correlation of strong earthquakes with radiation belt particle flux variations. Geomagnetism and Aeronomy 34, 315–320 (English Translation).

Gokhberg, M.B., Gufeld, I.L., Rozhnoy, A.A., Marenko, V.F., Yampolsky, V.S., Ponomarev, E.A., 1989. Study of seismic influence on the ionosphere by super long-wave probing of the Earth-ionosphere waveguide. Physics of the Earth and Planetary Interiors 57, 64–67.

Grimalsky, V.V., Kremenetsky, I.A., Rapoport, Yu.G., 1999. Excitation of EMW in the lithosphere and propagation into magnetosphere. In: Hayakawa, M. (Ed.), Atmospheric and Ionospheric Electromagnetic Phenomena Associated with Earthquakes. TERRAPUB, Tokyo, pp. 777–787.

Guo, Z., Liu, B., Wang, Y., 1994. Mechanism of electromagnetic emissions associated with microscopic and macroscopic cracking in rocks. In: Hayakawa, M. (Ed.), Electromagnetic Phenomena Related to Earthquake Prediction. TERRAPUB, Tokyo, pp. 523–529.

Hayakawa, M., Kopytenko, Yu., Smirnova, N., Troyan, V., Peterson, Th., 2000. Monitoring ULF magnetic disturbances and schemes for recognizing earthquake precursors. Physics and Chemistry of the Earth (A) 25, 263–269.

Hayakawa, M., Molchanov, O.A., Nikolaenko, A.P., 2002. Model variations in atmospheric radio noise caused by preseismic modifications of tropospheric conductivity profile. In: Hayakawa, M., Molchanov, O.A. (Eds.), Seismo Electromagnetics: Lithosphere–Atmosphere–Ionosphere Coupling. TERRAPUB, Tokyo, pp. 349–352.

Henderson, T.R., Sonwalkar, V.S., Helliwell, R.A., Inan, U.S., Fraser-Smith, A.C., 1993. A search for ELF/VLF emissions induced by earthquakes as observed in the ionosphere by the DE-2 satellite. Journal of Geophysical Research 98, 9503–9514.

Ismaguilov, V.S., Kopytenko, Yu.A., Hattori, K., Voronov, P.M., Molchanov, O.A., Hayakawa, M., 2001. ULF magnetic emissions connected with under sea bottom earthquakes. Natural Hazards and Earth System Sciences 1, 23–31.

Johnston, M.J.S., 1997. Review of electric and magnetic fields accompanying seismic and volcanic activity. Surveys in Geophysics 18, 441–475.

Johnston, M.J.S., Mueller, R.J., 1987. Seismomagnetic observations during the 8 July 1986 magnitude 5.9 North Palm Springs earthquake. Science 237, 1201–1203.

Kopytenko, Yu.A., Matiashvili, T.G., Voronov, P.M., Kopytenko, E.A., Molchanov, O.A., 1993. Detection of ultra-low-frequency emissions connected with the Spitak earthquake and its aftershock activity, based on geomagnetic pulsations data at Dusheti and Vardzia observatories. Physics of the Earth and Planetary Interiors 77, 85–95.

Krechetov, V.V., 1996. Cerenkov radiation of protons in the magnetosphere as a source of VLF waves preceding an earthquake. Geomagnetism and Aeronomy 35, 688–691 (English Translation).

Larkina, V.I., Migulin, V.V., Molchanov, O.A., Kharkov, I.P., Inchin, A.S., Schvetsova, V.V., 1989. Some statistical results on very low frequency radiowave emissions in the upper ionosphere over earthquake zones. Physics of the Earth and Planetary Interiors 57, 100–109.

Lee, C.C., Liu, J.Y., Pan, C.J., 2000. The height of sporadic-E layer simultaneously observed by the VHF radar and ionosondes in Chung-Li. Geophysical Research Letters 27, 641–644.

Lennard, M.H., Mazur, J.E., Mason, G.M., 2000. SAMPEX Level-2 Data Products NSSDC Submission Description. University of Maryland, Maryland.

Marshall, A.W., Olkin, I., 1979. Inequalities: Theory of Majorization and its Applications. Academic Press, New York.

Merzer, M., Klemperer, S.L., 1997. Modeling low-frequency magnetic-field precursors to the Loma Prieta earthquake with a precursory increase in fault-zone conductivity. Pure and Applied Geophysics 150, 217–248.

Molchanov, O.A., Hayakawa, M., 1998. On the generation mechanism of ULF seismogenic electromagnetic emissions. Physics of the Earth and Planetary Interiors 105, 201–210.

Molchanov, O.A., Mazhaeva, O.A., Golyavin, A.N., Hayakawa, M., 1993. Observation by the Intercosmos-24 satellite of ELF-VLF electromagnetic emissions associated with earthquakes. Annales Geophysicae 11, 431–440.

Molchanov, O.A., Hayakawa, M., Rafalsky, V.A., 1995. Penetration characteristics of electromagnetic emissions from an underground seismic source into the atmosphere, ionosphere and magnetosphere. Journal of Geophysical Research 100, 1691–1712.

Myachkin, V.I., Brace, W.F., Sobolev, G.A., Dieterich, J.H., 1975. Two models for earthquake forerunners. Pure and Applied Geophysics 113, 169–181.

Nitsan, U., 1977. Electromagnetic emission accompanying fracture of quartz-bearing rocks. Geophysical Research Letters 4, 333–336.

Ohta, K., Umeda, K., Watanabe, N., Hayakawa, M., 2001. ULF/ELF emissions observed in Japan, possibly associated with the Chi-Chi earthquake in Taiwan. Natural Hazards and Earth System Sciences 1, 37–42.

Oike, K., Ogawa, T., 1986. Electromagnetic radiations from shallow earthquake observed in the LF range. Journal of Geomagnetism and Geoelectricity 38, 1031–1040.

Park, S.K., Johnston, M.J.S., Madden, T.R., Morgan, F.D., Morrison, H.F., 1993. Electromagnetic precursors to earthquakes in the ULF band: a review of observations and mechanisms. Reviews of Geophysics 31, 117–132.

Parrot, M., 1994. Statistical study of ELF/VLF emissions recorded by a low-altitude satellite during seismic events. Journal of Geophysical Research 99, 23339–23347.

Parrot, M., 1999. Statistical studies with satellite observations of seismogenic effects. In: Hayakawa, M. (Ed.), Atmospheric and Ionospheric Electromagnetic Phenomena Associated with Earthquakes. TERRAPUB, Tokyo, pp. 685–695.

Parrot, M., 2002. The micro-satellite DEMETER. Journal of Geodynamics 33, 535–541.

Parrot, M., Mogilevsky, M.M., 1989. VLF emissions associated with earthquakes and observed in the ionosphere and the magnetosphere. Physics of the Earth and Planetary Interiors 57, 86–99.

Parrot, M., Achache, J., Berthelier, J.J., Blanc, E., Deschamps, A., Lefeuvre, F., Menvielle, M., Plantet, J.L., Tarits, P., Villain, J.P., 1993. High frequency seismo-electromagnetic effects. Physics of the Earth and Planetary Interiors 77, 65–83.

Picozza, P. (PAMELA/ARINA collaboration), 2003. The PAMELA MISSION. http://wizard.roma2.infn.it/pamela/index.htm

Pulinets, S.A., Boyarchuk, K.A., Hegai, V.V., Kim, V.P., Lomonosov, A.M., 2000. Quasielectrostatic model of atmosphere–thermosphere–ionosphere coupling. Advances in Space Research 26, 1209–1218.

Pustovetov, V.P., Malyshev, A.B., 1993. Space–time correlation of earthquakes and high-energy particle flux variations in the inner radiation belt. Cosmic Research 31, 84–90.

Rodger, C.J., Dowden, R.L., Thomson, N.R., 1999. Observations of electromagnetic activity associated with earthquakes by low-altitude satellites. In: Hayakawa, M. (Ed.), Atmospheric and Ionospheric Electromagnetic Phenomena Associated with Earthquakes. TERRAPUB, Tokyo, pp. 697–710.

Rudemo, M., 1982. Empirical choice of histograms and Kernel density estimators. Scandinavian Journal of Statistics 9, 65–78.

Scott, D.W., 1992. Multivariate Density Estimation. Wiley, New York, pp. 76–80.

Serebryakova, O.N., Bilichenko, S.V., Chmyrev, V.M., Parrot, M., Rauch, J.L., Lefeuvre, F., Pokhotelov, O.A., 1992. Electromagnetic ELF radiation from earthquake regions as observed by low-altitude satellite. Geophysical Research Letters 19, 91–94.

Sgrigna V. (ESPERIA collaboration), 2001. ESPERIA Phase A Report, ASI Program for Small Scientific Missions, pp. 1–198.

Sgrigna, V., Malvezzi, V., 2003. Preseismic creep strains revealed by ground tilt measurements in central Italy on the occasion of the 1997 Umbria-Marche Apennines earthquake sequence. Pure and Applied Geophysics 160, 1493–1515.

Sgrigna, V., D'Ambrosio, C., Yanovskaya, T.B., 2002a. Numerical modeling of preseismic slow movements of crustal blocks caused by quasi-horizontal tectonic forces. Physics of the Earth and Planetary Interiors 129, 313–324.

Sgrigna, V., Console, R., Conti, L., Galper, A., Malvezzi, V., Parrot, M., Picozza, P., Scrimaglio, R., Spillantini, P., Zilpimiani, D., 2002b. Preseismic natural emissions from the Earth's surface and their effects in the near Earth space. A project for monitoring earthquakes from space. EOS Transactions, AGU 83 (19), S356 (T22B-10).

Simonoff, S.J., Frederic, U., 1997. Measuring the stability of histogram appearance when the anchor position is changed. Comparative Statistics and Data Analysis 23, 335–353.

Smirnova, N.A., 1999. The peculiarities of ground-observed geomagnetic pulsations as the background for detection of ULF emission of seismic origin. In: Hayakawa, M. (Ed.), Atmospheric and Ionospheric Electromagnetic Phenomena Associated with Earthquakes. TERRAPUB, Tokyo, pp. 215–232.

Sorokin, V.M., Chmyrev, V.M., Yaschenko, A.K., 2001. Electrodynamic model of the lower atmosphere and the ionosphere coupling. Journal of Atmospheric and Solar-Terrestrial Physics 63, 1681–1691.

Surkov, V., 1999. ULF electromagnetic perturbations resulting from the fracture and dilatancy in the earthquake preparation zone. In: Hayakawa, M. (Ed.), Atmospheric and Ionospheric Electromagnetic Phenomena Associated with Earthquakes. TERRAPUB, Tokyo, pp. 371–382.

Teisseyre, R., 1997. Generation of electric field in an earthquake preparation zone. Annali di Geofisica 40, 297–304.

USGS catalog, 2003, www.usgs.gov.

Uyeda, S., Sulaiman Al-Damegh, K., Dologlou, E., Nagao, T., 1999. Some relationship between VAN seismic electric signals (SES) and earthquake parameters. Tectonophysics 304, 41–55.

Varotsos, P., Alexopoulos, K., Lazaridou, M., Nagao, 1993. Earthquake predictions issued in Greece by seismic electric signals since February 6, 1990. Tectonophysics 224, 269–288.

Varotsos, P., Sarlis, N., Lazaridou, M., Kapiris, P., 1997. Transmission of stress induced electric signals in dielectric media. Journal of Applied Physics 83, 60–70.

Voronov, S.A., Galper, A.M., Koldashov, S.V., Maslennikov, L.V., Mikhailov, V.V., Nikitina, N.V., Popov, A.V., 1990. Increases in high energy charged particle fluxes near the South Atlantic Magnetic Anomaly and the seismicity of the Earth. Cosmic Research 28, 789–791.

Walt, M., 1994. Introduction to Geomagnetically Trapped Radiation. Cambridge University Press, Cambridge.

Warwick, J.W., Stoker, C., Meyer, T.R., 1982. Radio emission associated with rock fracture: possible application to the great Chilean earthquake of May 22, 1960. Journal of Geophysical Research 87, 2851–2859.

Yoshida, S., Uyeshima, M., Nakatani, M., 1997. Electric potential changes associated with slip failure of granite: preseismic and coseismic signals. Journal of Geophysical Research 102, 14883–14897.